Microstructural and Mineralogical Analysis of Alkali Activated Fly Ash-Slag Pastes

Nedeljkovic, Marija; Arbi Ghanmi, Kamel; Zuo, Yibing; Ye, Guang

Microstructural and Mineralogical Analysis of Alkali Activated Fly Ash-Slag Pastes

Marija Nedeljković (1), Kamel Arbi (1), Yibing Zuo (1) and Guang Ye (1)

(1) Materials and Environment (Microlab), Faculty of Civil Engineering and Geosciences, Delft University of Technology, The Netherlands

Abstract

The performances of alkali activated materials (AAM) are strongly related to their microstructures. The microstructure development is mainly affected by chemistry of the primary raw materials. In the present study the influence of different proportions of fly ash and slag (100:0, 70:30, 50:50, 30:70, 0:100 wt.%, named S0, S30, S50, S70, S100, respectively) on the microstructure and mineralogy of the alkali activated fly ash and slag based pastes has been investigated through XRD, TGA/DTGA, ESEM/EDX techniques. XRD has been used for the qualitative and quantitative analysis of different reaction products.

The Rietveld refinement method and TGA/DTGA analysis have demonstrated that the increase of slag content increased the amount of amorphous phase associated with gel formation. From ESEM results, a more refined and denser matrix has been deduced in slag rich mixtures. These results are in agreement with higher strength values observed for S70 and S100 mixtures (~100 MPa at 28d and ~120 MPa after 90d curing). Depending on the fly ash to slag ratio, two types of gel have been distinguished by EDX analysis, a N-A-S-H gel in the fly ash rich mixtures and a C-A-S-H gel in the slag rich pastes.

Keywords: Alkaline activation; Fly ash; Slag; Gel composition; Mineralogy

1. INTRODUCTION

The energy consumption, CO_2 gas emission and depletion of natural's resources are the three main constraints in cement technology and the building industry. The total CO_2 footprint per ton of Portland cement is almost 1:1, meaning that for each ton of Portland cement produced, approximately one ton of CO_2 is emitted [1]. In order to build sustainable constructions, alternative technology such as alkaline activation appears to fit well criteria for the design of environmental friendly concrete with similar properties to these of the Portland cement concrete. The design is based on alkaline activation of by-products from the industrial processes, such as fly ash (FA) and blast furnace slag (BFS). Their activation rate depends on the type of alkaline cation, the presence of soluble elements in the activator, amorphous phase content in the raw material, water to binder ratio and curing conditions. The production of the single systems such as alkali activated fly ash (AAFA) or alkali activated slag (AAS) have many challenges, such as required thermal curing at the early age of AAFA or drying shrinkage of AAS since the slag consumes more water compared to ordinary Portland cement or fly ash. The use of blended systems of fly ash and slag shows to be more beneficial for development of more stable microstructure with better properties [2-5]. However, the development of the microstructure in the blended systems of alkali activated fly ash and slag varies together with slag content and alkaline solution used.

Blended mixtures can provide more stable systems, with moderate reaction rate, reduced porosity, less brittleness such existing in slag systems, low stresses due to material deformations, e.g. shrinkage. It is believed that the replacement of fly ash with slag is beneficial to the certain range [5]. However, studies on mechanical and microstructural level in order to investigate that effect are fairly limited. Therefore, identification of the suitable ratios between fly ash and slag requires study on microstructural evolution combined with mechanical properties of their blends.

This paper presents a study on this effort. The microstructure, mineralogical composition and mechanical properties of alkali activated FA and BFS pastes are investigated with respect to their different ratios in the mixtures. The curing age of 28 days has been chosen for the micro structural analysis, since most of the mechanical strength is developed at this age. The following analytical techniques have been used for characterization: XRD, TGA/DTGA, SEM-EDX. The most striking differences between fly ash, blast furnace slag and their blended systems will be discussed.

2. MATERIALS AND METHODS

2.1 Materials and sample preparations

The precursors used in this study were fly ash and blast furnace slag. The chemical compositions of the precursors were determined by XRF (Table 2.1). The mineral composition was measured using powder X-ray diffraction (Fig.1). Blast furnace slag was almost fully amorphous, while fly ash was partially with crystalline phases such as quartz, mullite and hematite. The alkali activator was prepared by mixing two solutions the sodium hydroxide and sodium silicate. The activator was cooled down after mixing to room temperature prior to preparation of the pastes. The liquid to solid mass ratio (l/s) was 0.4, which gave a suitable workability. Pastes were produced with the following ratios of fly ash and slag, 100:0, 70:30, 50:50, 30:70, 0:100 wt%, named S0, S30, S50, S70, S100. They were dry-mixed for 3 minutes to get homogeneous precursor and then mixed with the activator.

The pastes were casted in prismatic moulds of 40x40x160 mm^3. The samples were demoulded 24 h after casting and further aged at an air-conditioned fog room at 22 ℃ and RH ~ 99%.

Table 2.1: Chemical compositions of FA and BFS deduced from X-ray fluorescence

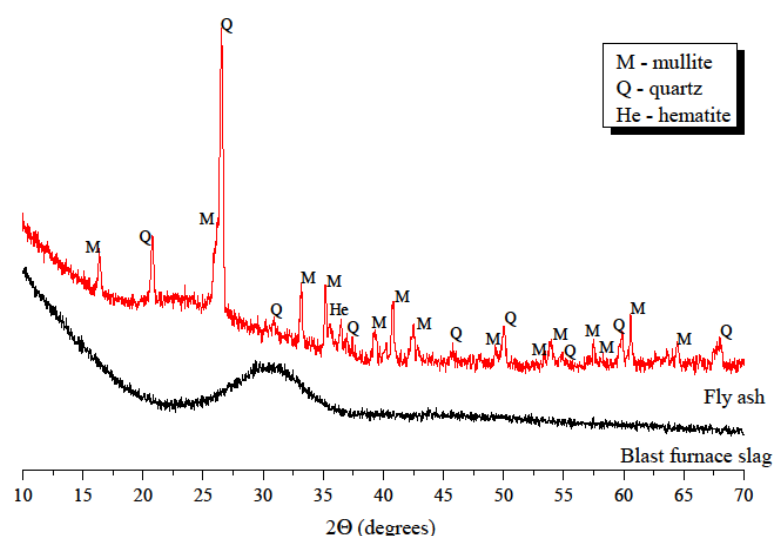|	SiO₂	Al₂O₃	CaO	MgO	Fe₂O₃	SO₃	Na₂O	K₂O	TiO₂	P₂O₅	L.O.I.
BFS	34.40	11.53	39.17	7.81	1.42	1.6	0.23	0.58	-	-	1.15
FA	54.28	23.32	4.23	1.62	8.01	0.64	0.85	1.97	1.23	0.54	3.37

Figure 1: XRD patterns of unreacted FA and BFS

2.2 Test methods

The flexural strength was measured using a standard three point bending test on 40x40x160 mm^3 prisms and the compressive strength test on 40x40x40 mm^3 cubes (NEN-EN-196-1).

X-ray diffraction was performed on finely ground paste powders with a step size of 0.02" for a 2θ angle range between 5 and 70 degrees. Every step was analyzed for 10 seconds. The Retvield refinement analysis was followed in order to quantify the content of different mineral phases present in alkali activated pastes. The internal standard method was used and a known amount (10 wt%.) of quartz (SiO₂) was chosen.

Thermogravimetric analysis/differential thermogravimetric analysis (TGA/DTGA) is carried out using a heating rate of 10 ℃/min between 40 ℃ and 1000 ℃, with an argon purge at 70 ml/min.

Environmental Scanning Electron Microscope (ESEM) Philips XL30 equipped with energy dispersive spectrometer (EDS) was used to collect images in backscattered electron detector (BSE) mode and to determine the qualitative composition of the reaction products. For the EDS analysis 30 individual values were collected from each sample.

3. RESULTS AND DISCUSSION

3.1 Mechanical properties

The flexural and compressive strengths (Fig. 2 and Fig. 3) were measured after 1, 7, 28, 90 and 270 days of curing at ambient temperature and 99% relative humidity. Two important relations should be noted, that the effect of fly ash/slag ratio on the development of strength and the tendency of the strength development depend on the timescale.

Fig 3. shows that the compressive strength increases at all ages for all pastes. Higher strength of alkali activated materials is associated with a higher fraction of aluminium rich structural units, higher rate of crosslinking, and more compact structure compared to cement based materials [6]. However, the strength development is more substantial in slag rich mixtures and at early age. This is in line with findings of Puertas et al. [7]. Higher slag content in the system increases dissolution rate and consequently hardening is faster, favouring high amount of the products forming within first few days of the reaction. The homogeneous distribution of the gel along with the small size and high connectivity of the units forming the gel in alkali activated slag paste is assumed to better distribute stress when the sample is under load, resulting in the compressive strength of S100 paste ~100 MPa at 28d and ~120 MPa after 90d curing (Fig. 3). Conversely, the less homogeneous distribution of material and more porous microstructure of fly ash rich mixtures resulted in higher local stress concentration under load and lower ultimate strength (Fig.3).

When fly ash was replaced by 30 wt.% of slag or more, the strength was increased clearly indicating the reactivity of the fly ash/slag blended system. Presence of slag in the system either at low, moderate or high percentage favours the geopolymerization reactions and accelerates hardening process, which is in line with previous results [7]. It can be noticed from Fig. 3 that curing for 28 and 90 days has not made significant difference in the developed compressive strength for those ages, suggesting that main bearing phases of strength have been produced before 28 days curing. The strength at 270 days for slag rich mixtures showed that there was not any increase of strength. Instead, for those mixtures strength was slightly declined. However, for fly ash rich paste, i.e. S30 the strength has increased, suggesting that unhydrated material is reacting at later ages.
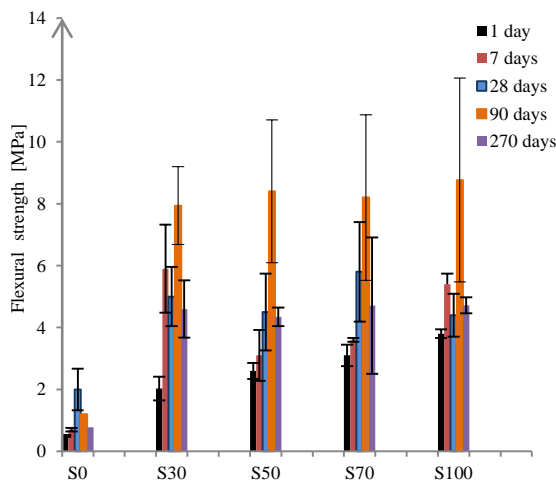

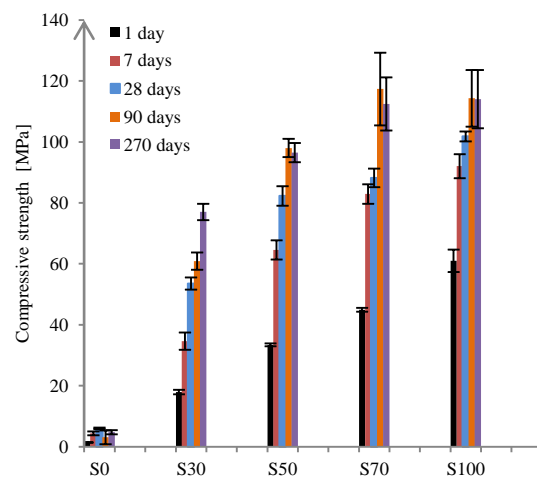Figure 2: Flexural strengths of alkali activated fly ash/slag pastes at different ages

Figure 3: Compressive strengths of alkali activated fly ash/slag pastes at different ages

The influence of different fly ash/slag ratio on the flexural strength is not clear. It can be observed from Fig. 2 that flexural strengths at 28 and 90 days are almost the same for all tested mixtures except S0, while at 270 days the flexural strength has decreased for half compared to 90 days. It is known that the mean chain length (MCL) and Ca/Si ratio have significant effect on the mechanical properties of the gel [11]. Therefore, in this work is assumed that MCL has primary effect on the response of the material to flexural loading. In general, MCL is defined as the number of aluminosilicate tetrahedra per tobermorite chain in the gel of alkali activated slag rich binders [11]. Since the MCL is related to the amount of alumina and silica units, plotting relationship between SiO_2 and Al_2O_3/SiO_2 for different mixtures from EDS analysis in this work, it can be seen that the increase of slag in the system decreases SiO_2 content where ratio Al_2O_3/SiO_2 decreases too, but negligibly (Fig. 4). It can be concluded that MCL for different mixtures will not be changed significantly. Therefore, this can be one of the possible reasons for similar flexural strength values of the studied mixtures.
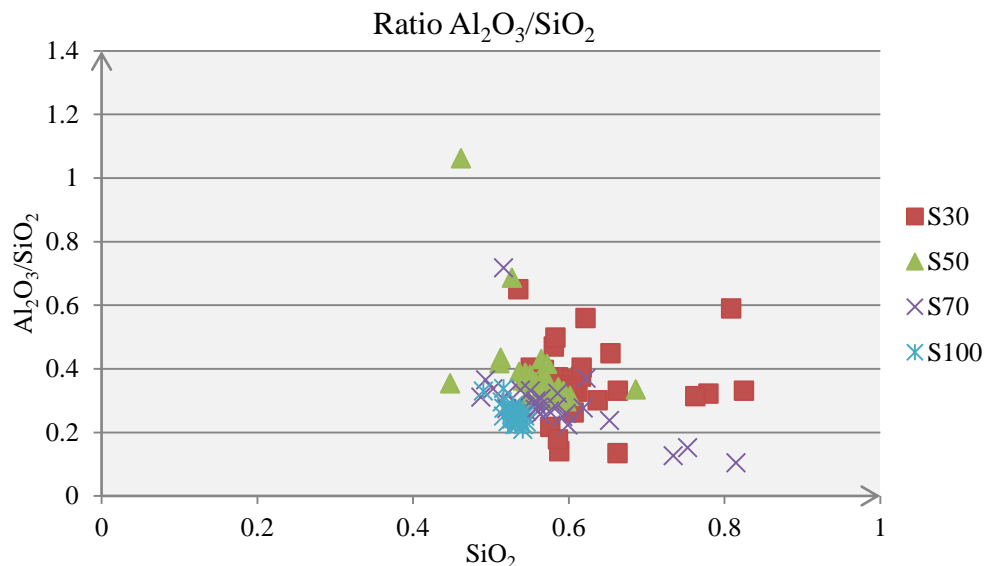

Figure 4: SiO_2 vs Al_2O_3/SiO_2 for alkali activated pastes at 28 days

3.2 X-ray diffraction, Rietveld analysis

The 28 days cured samples consist of gel, unreacted fly ash and unreacted slag particles (Fig. 8). The shift of hump between 15 and 30 ° in the S0 sample indicates the sodium aluminate silicate hydrate (N-A-S-H) gel formation. The calcium aluminate silicate hydrate (C-A-S-H) phase identified around 29.4 ° was the main reaction product in the samples with 30 wt%. and higher slag amount (Fig.5). In addition, the traces of katoite $(Ca_3Al_2(SiO_4)_{3-x}(OH)_{4x}$ and vaterite were found between 32-34 ° in the sample S100 (Fig. 5). Amorphous phases cause a rather high background or broad peaks such as in the pastes S50, S70 and S100, suggesting high content of the amorphous gel in the material. This is confirmed by the quantitative phase analysis which was done by the Rietveld method. From the results shown in the Fig 6, it can be observed that amorphous phases comprised the majority, nearly 70% of the sample. The amorphous phase is assigned to amorphous part in the reacted and unreacted material, where only reacted amorphous part indicates strength gain. The studied material is highly reactive and the high compressive strength (Fig. 3) can be

justified by amorphous phase proportion in the total binder per sample (Fig. 6). The phase analysis reveals that amount of amorphous phase enabled maximizing early strength in slag rich samples and later strength in fly ash rich samples to achieve the materials full strength potential under the adopted alkaline activation conditions (Fig. 3).
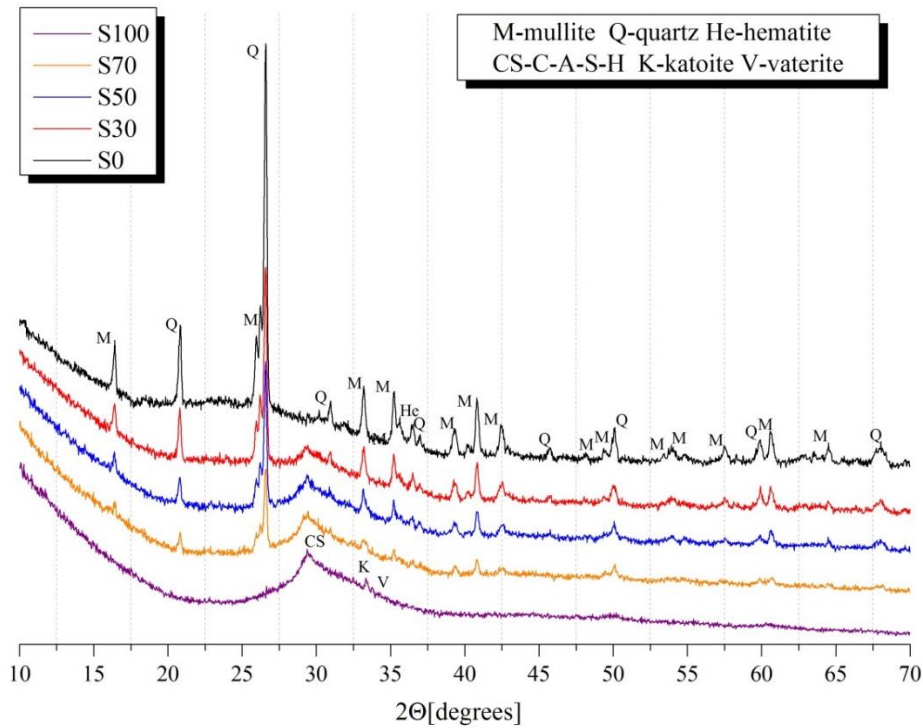

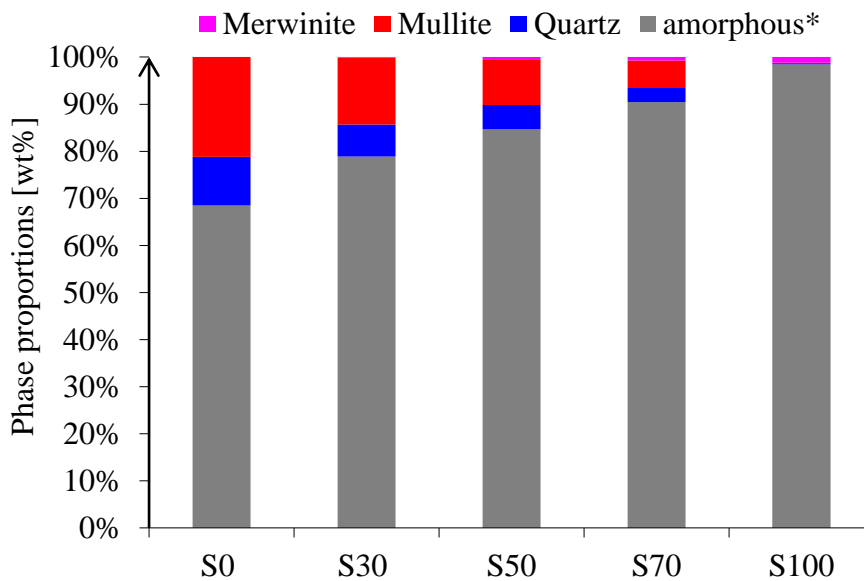Figure 5: XRD spectrums of the alkali activated fly ash and slag pastes at 28 days

Figure 6. XRD quantification of different phases formed in S0, S30, S50, S70, S100, respectively at 28 days

3.3 Thermogravimetric analysis (TGA/DTGA)

Gel formation has been examined by thermogravimetric and differential thermogravimetric analysis (TGA/DTGA). The mass losses between 40 ℃ and 700 ℃ were assigned to the combined dehydration and dehydroxylation effects of C-A-S-H, katoite, Al(OH)$_3$ and AFm phases which is in agreement with [9]. The samples were freeze-dried and equilibrated to ~30% RH to remove the capillary and gel water prior to TGA tests. The C-A-S-H gel is the dominant reaction product in the studied mixtures, excluding S0 sample where N-A-S-H gel is formed according to X-ray diffraction results discussed in section 3.2. Plotted DTGA curves for the studied mixtures have similar peaks centred at 100-150 ℃ suggesting formation of the comparable reaction products. Furthermore, TGA curves (Fig.7 (a)) indicate that >80% of the total mass loss in each sample is from interlayer and structurally bound water either in N-A-S-H or C-A-S-H gel within the temperature range from 105 to 400 ℃.
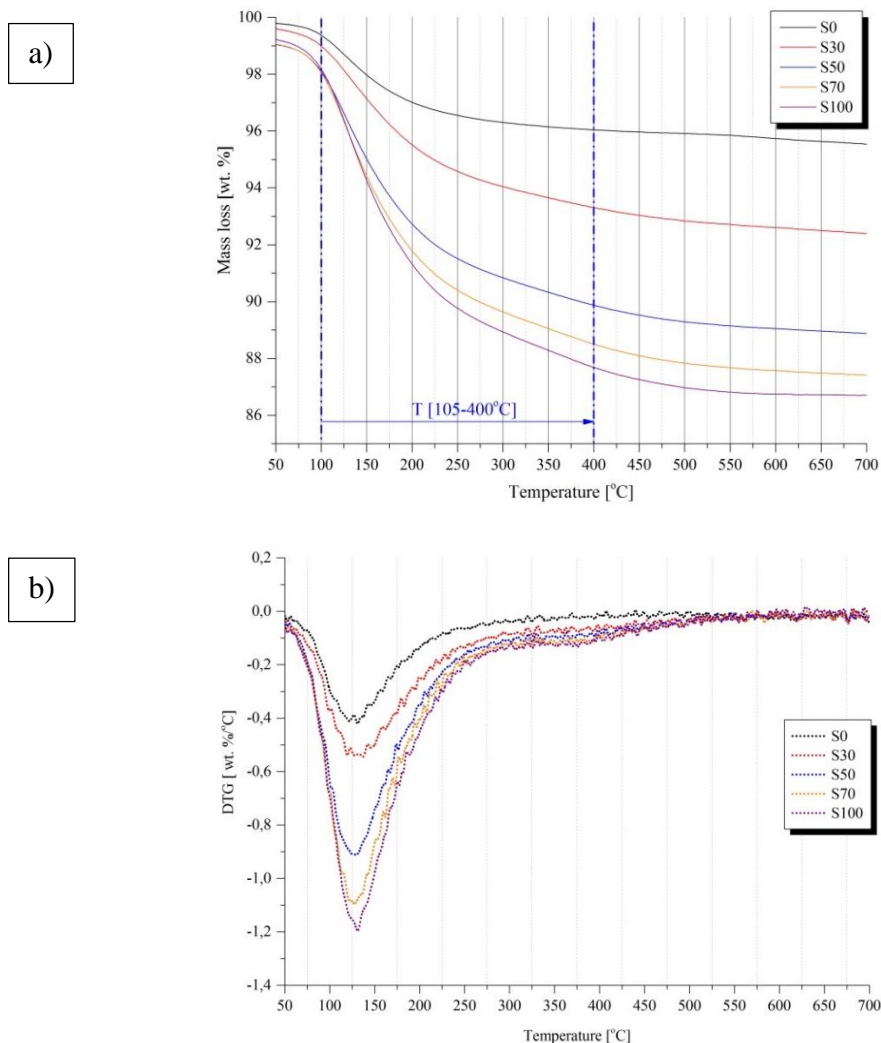

Figure 7. TGA spectra (a) and DTGA (b) of the alkali activated fly ash and slag pastes at 28d

The total mass loss of the reaction products was determined from the TGA curves (Fig.7. (a)). It is assumed that in the temperature range from 105 to 400 ℃, the mass loss corresponds to the dehydration process of amorphous gel phases. The results are shown in the

table 3.1. Mass loss is increasing relatively to the increase of slag in the system. Therefore, mixture S100 has the highest mass loss suggesting high gel content, which is consistent with the Rietveld refinement results where the most gel amount formed was found in S100.

Table 3.1 Mass loss in alkali activated pastes at 28 days

Mixture	S0	S30	S50	S70	S100
Mass loss [%]	2.95	4.81	7.02	8.14	8.96

3.4 Environment Scanning electron microscopy (ESEM) and Energy dispersive X-ray diffraction (EDX) analysis

Microscopic examination of 28 days cured samples is presented in Fig. 8. The BSE image of alkali activated fly ash paste S0 shows a highly heterogeneous and porous microstructure with different sizes of spherical unreacted fly ash particles. Some particles are intact or interconnected with other spheres. This microstructure is consistent with the limited mechanical strength (Fig. 3). Increasing the slag content, a more homogeneous and dense matrix is formed and the compressive strength values are consequently improved. The microstructure mainly consists of space-filling C-A-S-H type gel, as identified by XRD and TGA analysis. The amounts of Al, Si, Ca, Mg in atomic-% within the binder regions (excluding unreacted FA and BFS) were obtained from EDS spectra. The effect of studied fly ash/slag ratios on gel chemistry is performed by $CaO-SiO_2-Al_2O_3$ and $CaO-Al_2O_3-MgO$ ternary diagrams. Calcium, aluminium, silicon and magnesium contents in the samples were renormalized to 100% on an oxide basis, excluding all other elements present in the samples. In addition, the atomic ratios Mg/Si vs Al/Si results are presented in the graphs for multiple points (Fig. 11).

The main reaction products is N-A-S-H gel in alkali activated fly ash paste according to plotted points in the ternary diagram (Fig. 9) where CaO content is close to zero. On the other hand, the main reaction products in alkali activated pastes that contain slag is C-A-S-H gel with modifications in chemical composition of present oxides across the different slag/fly ash pastes. The Al_2O_3 content [0.1-0.2] and SiO_2 content [0.5-0.6] of the pastes has not change significantly at different fly ash/slag ratios (Fig. 9). On the other hand, CaO content [0.15-0.35] is increasing with slag content increase in the mixtures, which clearly indicates the variation in gel composition as a function of CaO content (Fig 9). The pastes with 50, 70 and 100 % wt. slag have the gel of very uniform composition since all points are closely clustered as shown in Fig.9.

Fig. 11 shows correlation of Mg/Si with Al/Si. The slope of the plot in sample S100 indicates the Mg/Al ratio of hydrotalcite, which was not identified by X-ray diffraction. Therefore, this phase is either disordered or included in the main reaction products as it can be seen from the relation between $CaO-Al_2O_3-MgO$ in ternary diagram (Fig. 10). It is also assumed that crystalline hydrotalcite forms in later curing age and 28 days is not enough for its maturing and identification by X-ray diffraction.
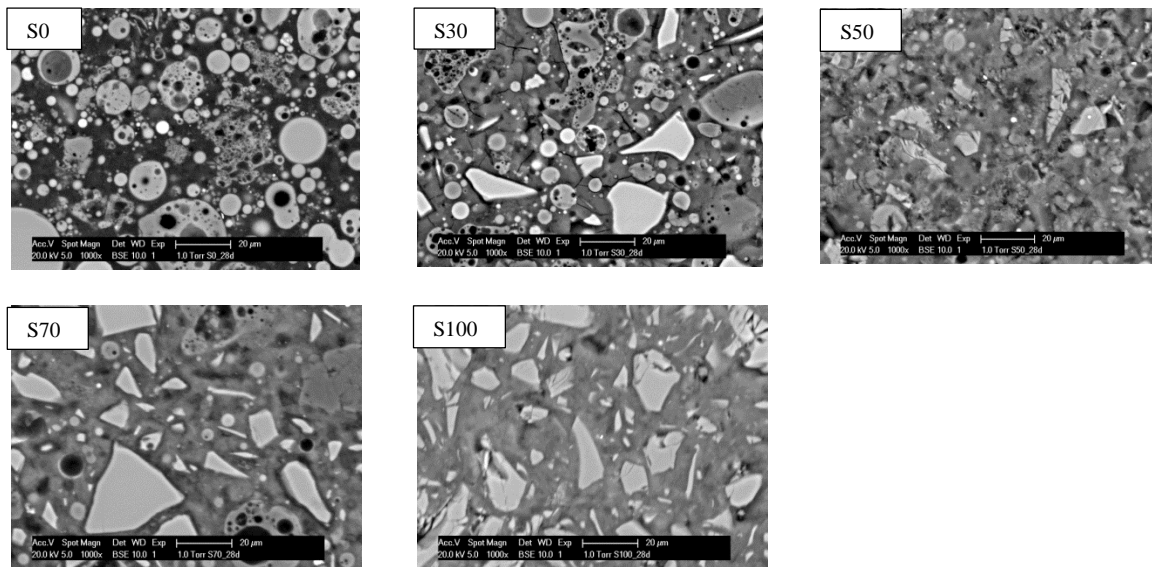
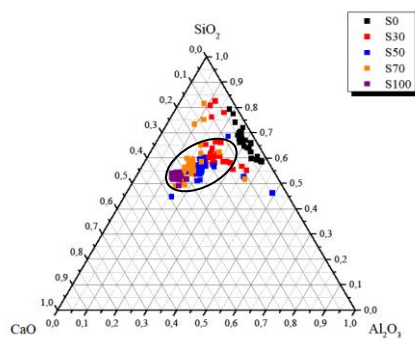Figure 8: BSE images of alkali activated pastes at 28 days

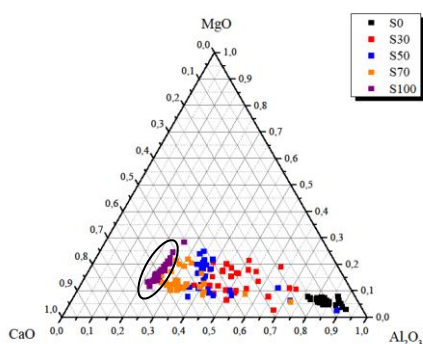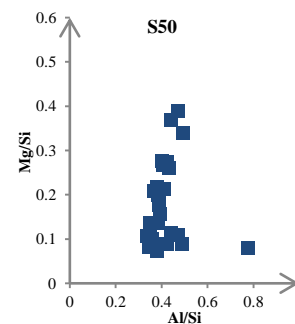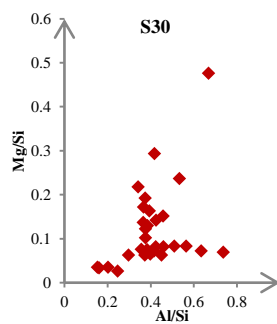Figure 9: Ternary diagram of CaO-Al$_2$O$_3$-SiO$_2$ as a function of slag replacement level

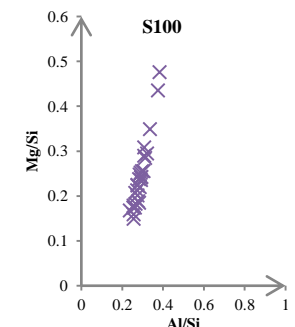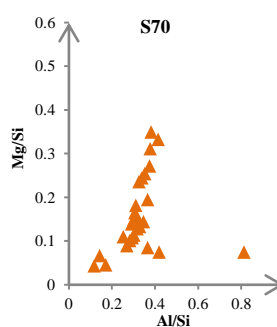Figure 10: Ternary diagram of CaO-Al$_2$O$_3$-MgO as a function of slag replacement level

Figure 11: Atomic Mg/Si vs Al/Si for alkali activated pastes at 28 days

4. CONCLUSIONS

The findings in this study showed that the high-strength alkali activated composite can be produced by using only a low to moderate-concentrated activator which could reduce both the

CO_2 emission and cost of the manufacturing processes. The slag use in the binder resulted in significant microstructural densification leading to high mechanical properties (more than 100 MPa in slag rich samples). The formation of more compact and uniform matrix leads to higher compressive strength associated with C-A-S-H gel formation for higher slag content (>50 wt%). A high amorphous phase content (>70%) was determined in all investigated mixtures, where the main amorphous phase was detected by widened hump assigned to the C-(A-)-S-H gel and also possible to N-A-S-H gel. The combined fly ash and slag counterbalance their properties giving more uniform development of the microstructure. Therefore, the optimal properties of studied alkali-activated pastes (compressive strength, amorphous phase content, gel microanalysis) can be captured already in the S50 paste.

ACKNOWLEDGEMENTS

REFERENCES

[1] Arbi, K., Nedeljkovic, M., Zuo, Y. and Ye, G. 'A Review on the Durability of Alkali-Activated Fly Ash/Slag Systems: Advances, Issues, and Perspectives', Ind. Eng. Chem. Res. 55 (19) (2016) 5439-5453.

[2] Ismail, I., Bernal, S. A., Provis, J. L., San Nicolas, R., Hamdan, S. and van Deventer, J. S. J. 'Modification of phase evolution in alkali-activated blast furnace slag by the incorporation of fly ash', Cem. Concr. Compos. 45, 125-135.

[3] Garcia-Lodeiro, I., Palomo, A., Fernández-Jiménez, A., and Macphee, D. E., 'Compatibility studies between NASH and CASH gels. Study in the ternary diagram Na2O–CaO–Al2O3–SiO2–H2O', Cem. Concr. Res. 41 (9) (2011) 923-931.

[4] Zhao, F. Q., Ni, W., Wang, H. J. and Liu, H. J., 'Activated fly ash/slag blended cement', Resour. Conserv. Recycl. 52 (2) (2007) 303-313.

[5] Hong, S. Y., and Glasser, F. P., 'Alkali sorption by CSH and CASH gels: Part II. Role of alumina', Cem. Concr. Res. 32 (7) (2002) 1101-1111.

[6] Marjanović, N., Komljenović, M., Baščarević, Z., Nikolić, V., and Petrović, R., Physical–mechanical and microstructural properties of alkali-activated fly ash–blast furnace slag blends, Ceram. Int. 41 (1) (2015) 1421-1435.

[7] Puertas, F., Martínez-Ramírez, S., Alonso, S., and Vazquez, T., 'Alkali-activated fly ash/slag cements: strength behaviour and hydration products', Cem. Concr. Res. 30 (10) (2000), 1625-1632

[8] Palomo, A., Grutzeck, M. W. and Blanco, M. T., 'Alkali-activated fly ashes: a cement for the future', Cem. Concr. Res. 29 (8) (1999), 1323-1329.

[9] Lothenbach, B. and Gruskovnjak, A., 'Hydration of alkali-activated slag: thermodynamic modelling', Adv. Cem. Res. 19 (2) (2007) 81.

[10] Bernal, S. A., Provis, J. L., Walkley, B., San Nicolas, R., Gehman, J. D., Brice, D. G., and van Deventer, J. S., 'Gel nanostructure in alkali-activated binders based on slag and fly ash, and effects of accelerated carbonation', Cem. Concr. Res. 53 (2013) 127-144.

[11] Myers, R. J., Bernal, S. A., San Nicolas, R. and Provis, J. L., 'Generalized structural description of calcium–sodium aluminosilicate hydrate gels: the cross-linked substituted tobermorite model', Langmuir, 29 (17) (2013) 5294-5306.